Enhanced specific capacitance and electrochemical properties of nickel hydroxide-activated carbon (α-Ni(OH)$_2$–AC) nanocomposite for pseudocapacitor electrode material

Sachin B. Abitkar[1,2], Suprimkumar D. Dhas[2], N. P. Jadhav[3], Pravin R. Jadhav[3], Parvejha S. Maldar[2], C. E. Patil[1], and Annasaheb V. Moholkar[2,*] (iD)

[1] *Department of Physics, Dr. Patangrao Kadam Mahavidyalaya, Sangaliwadi, Sangali, M.S. 416416, India*
[2] *Thin Film Nanomaterials Laboratory, Department of Physics, Shivaji University, Kolhapur, M.S. 416004, India*
[3] *Department of Physics, Devchand College, Arjunnagar, M.S. 591269, India*

ABSTRACT

Hierarchical mesoporous nickel hydroxide (α-Ni(OH)$_2$) nanoparticles have been prepared by an inexpensive, simple, and green co-precipitation technique. The α-Ni(OH)$_2$-activated carbon (AC) composite films have been fabricated onto a stainless steel substrate by the doctor blade method through the incorporation of AC into α-Ni(OH)$_2$ nanoparticles. The electrochemical performance of the composite electrode material is evaluated by varying the concentration of AC in the composite. As compared to pure α-Ni(OH)$_2$, the α-Ni(OH)$_2$–AC composite exhibits a more specific capacitance of 436 Fg^{-1} and noteworthy long-term capacitance retention of 81% after 1500 cycles. The α-Ni(OH)$_2$–AC composite electrode materials will be the potential candidates for fabrication of next generation electrochemical supercapacitors.

1 Introduction

Because of higher specific power and long-term cyclic span mechanism, supercapacitor provides extensive use in different types of advanced energy storage applications. Based on the charging-discharging mechanism, supercapacitors are classified as electrochemical double-layer capacitors (EDLC), pseudocapacitors, and hybrid capacitors. However, in recent times, most of the research is centered on pseudocapacitors because of their high specific capacitance (C_{sp}) and long cyclic span [1, 2]. Generally, metal oxides/hydroxides are considered as suitable electrode materials for electrochemical capacitors [1].

Recently, transition metal hydroxide materials have been extensively investigated for fabricating electrochemical supercapacitors because of their unique properties like superior redox activity, high rate ability, and environmental friendliness [3]. But

---

Ⓐ Springer

low electrical conductivity of these materials leads to an unsatisfactory cycle stability, which restricts its use for energy storage applications. Therefore, fabricating a composite of metal hydroxide with carbonaceous material is an effective alternative to enhance its electrochemical performance [4]. Activated carbon (AC) is a popular carbonaceous material because of its high electrical conductivity, large surface area, eco-friendly character, and moderate cost [5, 6]. The metal oxides/hydroxides–AC composite have been used to develop the new generation supercapacitors to enhance the electrochemical performance of the metal oxides/hydroxides [5, 7]. A composite of metal oxides/hydroxides (MnO_2, Co_3O_4, RuO_2, ZnO, NiO, and $Ni(OH)_2$) with AC has already been used to improve the C_{sp} of pseudocapacitors [8–13].

Huang et al. [13] have synthesized $Ni(OH)_2$/AC composite electrode by a simple co-precipitation technique and showed the loading of $Ni(OH)_2$ with AC, to enhance the C_{sp} of composite electrodes. For the composite electrode, the C_{sp} was reported as 314.5 Fg^{-1}. Bhat et al. [14] have synthesized $Ni(OH)_2$ nanostructures with different morphologies such as nanosheets and microflowers by hydrothermal method and reported C_{sp} of 417 Fg^{-1} and 180 Fg^{-1} for the microflowers and nanosheets, respectively. Chang et al. [15] fabricated the $Ni(OH)_2$ electrodes by successive ionic layer adsorption and reaction method and investigated the effect of different electrolytes, concentrations of the electrolyte, deposited mass of the electrode material, and variation in the scan rates on the electrochemical properties of the $Ni(OH)_2$ electrodes. Park et al. [16] reported that, with an increase in current density, the addition of AC to $Ni(OH)_2$ was beneficial in preventing the decrement in C_{sp} of pure $Ni(OH)_2$ electrode material. Moreover, the C_{sp} of $Ni(OH)_2$/AC composite electrode was found to be two times more than pure AC-based EDLC electrochemical capacitors.

In the present work, α-$Ni(OH)_2$ nanoparticles have been synthesized via an eco-friendly co-precipitation method. The pure α-$Ni(OH)_2$, and α-$Ni(OH)_2$–AC composite films, are prepared by the doctor blade technique. The electrochemical performance of pure α-$Ni(OH)_2$, and α-$Ni(OH)_2$–AC composite films, is examined in 1 M KOH electrolyte. As prepared, α-$Ni(OH)_2$–AC composite electrode showed a notable electrochemical performance in 1 M KOH electrolyte. Moreover, the electrochemical performance of α-$Ni(OH)_2$–AC composite films is investigated by varying the concentration of AC in the composite.

2 Experimental details

2.1 Preparation of α-$Ni(OH)_2$ and α-$Ni(OH)_2$–AC composite films

The analytical reagent (AR) grade activated carbon (AC) powder was purchased from Loba Chemie Pvt. Ltd., Mumbai (India) and used without further purification. The AC powder was ball milled at 300 rpm for 24 h at room temperature. A co-precipitation technique was employed for the preparation of $Ni(OH)_2$ nanoparticles. For the synthesis of $Ni(OH)_2$ nanoparticles, 20 ml of 1 M nickel sulfate ($NiSO_4$·$6H_2O$) precursor solution and 15 ml of 0.25 M potassium persulfate ($K_2S_2O_8$) solution as an oxidizing agent were mixed in a beaker and agitated well to get a green homogeneous transparent solution. Aqueous ammonium hydroxide (NH_4OH) was used as a complexing agent. The NH_4OH solution was added to the green transparent solution, which resulted in the formation of brown-colored precipitates in the solution. The obtained precipitates were rinsed several times with a mixture of ethanol and double-distilled water. The precipitates were collected by filtering and then dried on a hot plate. After drying, the brown-colored $Ni(OH)_2$ nanoparticles were collected.

The mixture of 500 mg of as-prepared $Ni(OH)_2$ nanoparticles, 50 mg of polyvinylidene fluoride, and 25 mg of ball-milled AC powder, in N-methyl-2-pyrrolidone solvent, was ground in an agate mortar to generate an homogeneous paste. This paste was coated onto stainless steel (SS) substrate by the doctor blade technique. The deposited film was annealed at 300 °C for 30 min in a muffle furnace to remove the binders. Thus, obtained α-$Ni(OH)_2$–AC composite film was labeled as NAC-1.

The same procedure has been adopted by adding 50 mg, 75 mg, and 100 mg of AC powder with $Ni(OH)_2$ nanoparticles, and these prepared films were labeled as NAC-2, NAC-3, and NAC-4 composite films, respectively. Pure α-$Ni(OH)_2$ film was similarly fabricated by the doctor blade technique without adding AC powder. The loaded mass of the

🖄 Springer

active material onto the SS substrate was varying from 0.34 to 0.71 mg cm^{-2}.

2.2 Materials characterization

X-ray diffractometer (Bruker D2-Phaser) with Cu-Kα radiation (λ = 1.5406 Å) and Fourier transform infrared (FT-IR) spectroscopy (Bruker-Alpha II) were used to examine the phase identification and structural analysis of the α-Ni(OH)$_2$ nanoparticles and α-Ni(OH)$_2$–AC composites. The surface morphology of the pure α-Ni(OH)$_2$ and α-Ni(OH)$_2$–AC composite material was investigated by scanning electron microscopy (SEM) (JSM-6360). The surface area and pore size distribution of α-Ni(OH)$_2$–AC film were determined through Brunauer–Emmett–Teller (BET) and Barrett-Joyner-Halenda (BJH) analyses (Model-NOVA1000e Quantachrome). The electrochemical performance of the electrode materials was evaluated in 1 M KOH electrolyte by potentiostat PGSTAT302N (Metrohm Autolab, Netherlands). The standard three-electrode system comprising of α-Ni(OH)$_2$ and α-Ni(OH)$_2$–AC composite films as working electrodes, saturated calomel electrode (SCE) as a reference electrode, and graphite as a counter electrode was implemented for electrochemical measurements.

3 Results and discussion

3.1 X-ray diffraction (XRD) studies

Figure 1 displays the XRD patterns of (a) activated carbon (AC), (b) pure α-Ni(OH)$_2$, (c) NAC-1, (d) NAC-2, (e) NAC-3, and (f) NAC-4 composite films, respectively. For XRD pattern of pure α-Ni(OH)$_2$, the reflections observed at 11.6°, 23.7°, 33.4°, and 59.8° are indexed to (003), (006), (101), and (110) crystal planes, respectively, which confirms α-Ni(OH)$_2$ phase of Ni(OH)$_2$ nanoparticles (ICDD card No. 38-0715) [17, 18]. For the XRD pattern of AC, no strong reflections are observed, signifying the amorphous nature of AC [8]. In XRD patterns of α-Ni(OH)$_2$–AC composite (Fig. 1(c-f)) reflections observed at 12.4°, 33.2°, and 59.7° are assigned to (003), (101), and (110) crystal planes, respectively, which are very close to pure α-Ni(OH)$_2$ phase. It indicates that the α-Ni(OH)$_2$ is a predominant phase in the composite. Similar observations were
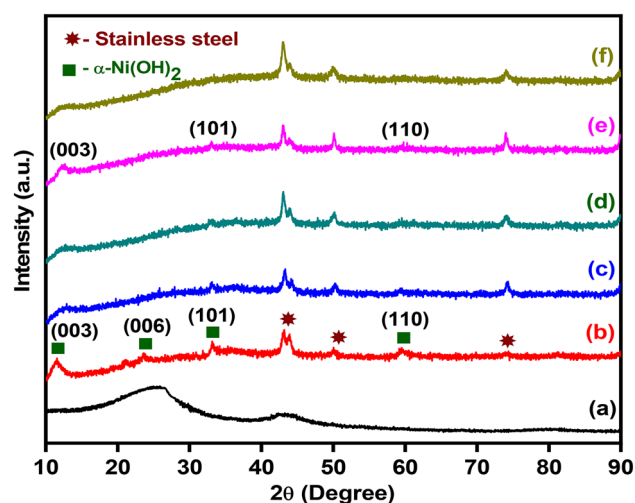

Fig. 1 X-ray diffraction patterns of (a) AC, (b) pure α-Ni(OH)$_2$ film, (c) NAC-1, (d) NAC-2, (e) NAC-3, and (f) NAC-4

previously reported by Tang et al. [18] for Ni(OH)$_2$/XC-72 composite.

The less intense reflections of the composite films indicate poor crystallinity of the composite material. The plausible reason for this may be the porous nature of the electrode materials. The porous nature of electrode material represents reduction in lattice energy and facilitates the rapid intercalation and deintercalation of electrolyte ions at the electrolyte–electrode surface [19]. Additionally, the reflections from the SS substrate are observed in the XRD patterns of both α-Ni(OH)$_2$ and α-Ni(OH)$_2$–AC composite, which are marked by symbol *.

3.2 FT-IR spectroscopy analysis

The FT-IR analysis of pure α-Ni(OH)$_2$ and α-Ni(OH)$_2$–AC composite was carried over a wavenumber range of 400–4000 cm^{-1} in KBr medium. Figure 2 reveals the FT-IR spectra of (a) pure α-Ni(OH)$_2$ film, (b) NAC-1, (c) NAC-2, (d) NAC-3, and (e) NAC-4 composite films, respectively. The FT-IR analysis helps to discover the nature of chemical bonds appearing in pure and composite materials. As shown in Fig. 2a, a broad band at 3445 cm^{-1} indicates the O–H stretching mode, and an intense band at 1631 cm^{-1} represents the O–H bending mode of H$_2$O molecules in the interlayer, which is in good agreement with reported by Gong et al. [3] and El-kermy et al. [20]. Besides, the intense absorption bands observed at 1121 cm^{-1}, 1040 cm^{-1}, and 927 cm^{-1} correspond to the interlayer-free sulfate ions [21]. A
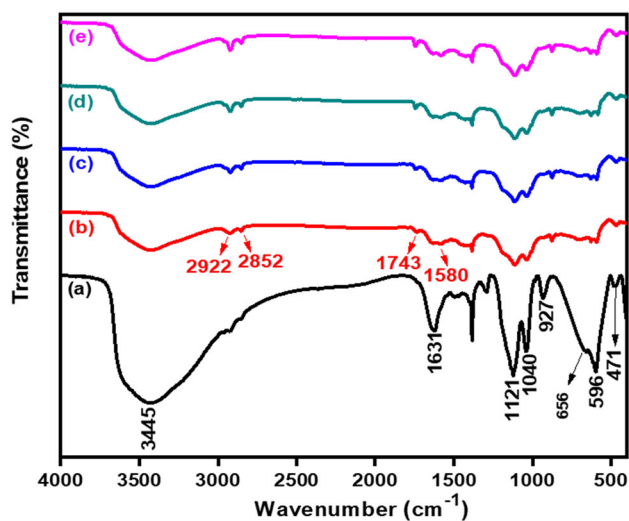
🖄 Springer

Fig. 2 FT-IR spectrum of (*a*) pure α-Ni(OH)$_2$ film, (*b*) NAC-1, (*c*) NAC-2, (*d*) NAC-3, and (*e*) NAC-4

band at 656 cm^{-1} is ascribed to the Ni–O–H stretching mode, which is a characteristic mode of α-Ni(OH)$_2$ [17, 22]. A strong band at 596 cm^{-1} is attributed to the existence of hydroxyl group [22, 23]. The stretching mode of Ni–O is confirmed by a less intense band centered at 471 cm^{-1} [20, 22]. The other less intense bands can be ascribed to the existence of carbonate ions, originating from atmospheric CO_2 absorption [17]. As shown in Fig. 2b–e, α-Ni(OH)$_2$–AC composite exhibits all the bands of α-Ni(OH)$_2$, but the presence of AC has shifted these bands to a lower wavenumber. Additionally, the bands appearing at 2922 cm^{-1} and 2852 cm^{-1} can be ascribed to the infrared C–H stretching vibrations from the AC surface. However, the intensity of these two bands is found to be reduced for pure α-Ni(OH)$_2$, the presence of these bands can be ascribed to infrared vibrations of CO_2 molecules which are absorbed from the atmosphere [21, 23, 24]. The bands observed at 1743 cm^{-1} and 1580 cm^{-1} are from the AC surface and can be assigned to C=O and C=C stretching vibrations, respectively [25, 26]. The intensity of the different bands of activated carbon in the composite films changes because of an increase in the concentration of activated carbon in the composite films. Thus, the FT-IR analysis reflected the presence of activated carbon in the composite, which signified the successful development of α-Ni(OH)$_2$–AC composite.

3.3 SEM studies

Figure 3a shows the SEM micrograph of pure α-Ni(OH)$_2$ film. The micrograph shows honeycomb-like interconnected nanowalls. The thickness of these nanowalls is roughly estimated as 40 nm. A similar type of morphology has been reported by Wu et al. [27] for nickel oxide/hydroxide electrodes. Figure 3b–e represent the surface morphology of NAC-1, NAC-2, NAC-3, and NAC-4, respectively. The surface morphology is composed of random distribution of sheets and flower-like microstructures with voids. Such type of morphology provides the enhanced surface area for the interaction of electrolyte ions across the electrolyte–electrode interface and improves the performance of electrochemical supercapacitors [13].

3.4 BET analysis

The specific surface area and pore size distribution of the NAC-2 composite were examined by the nitrogen adsorption–desorption isotherm. Figure 4 displays the nitrogen adsorption–desorption isotherm and the inset is pore size distribution. It is observed that the NAC-2 composite exhibit a large surface area of 211 m^{2}g^{-1}. The mean pore diameter is determined as 37 nm from the Barret–Joyner–Halenda (BJH) method.

3.5 Electrochemical studies

3.5.1 Cyclic voltammetric (CV) studies

The CV plots of pure α-Ni(OH)$_2$ and NAC-1, NAC-2, NAC-3, and NAC-4 composite films are shown in Fig. 5a, b–e, respectively, at a scan rate of 10 to 100 mVs^{-1} in 1 M KOH electrolyte. The potential window of 0 to 0.4 V vs. SCE was applied for the CV analysis of pure α-Ni(OH)$_2$ and α-Ni(OH)$_2$–AC composite films, respectively. The distinct redox peaks appeared in the CV plots of pure α-Ni(OH)$_2$ and composite films indicate the rapid redox reaction processes occurring at the electrolyte–electrode interface and represent the pseudocapacitive behavior of the composite electrode material [15, 28]. The redox reaction for the pure α-Ni(OH)$_2$ electrode material can be represented by the following Eq. (1).
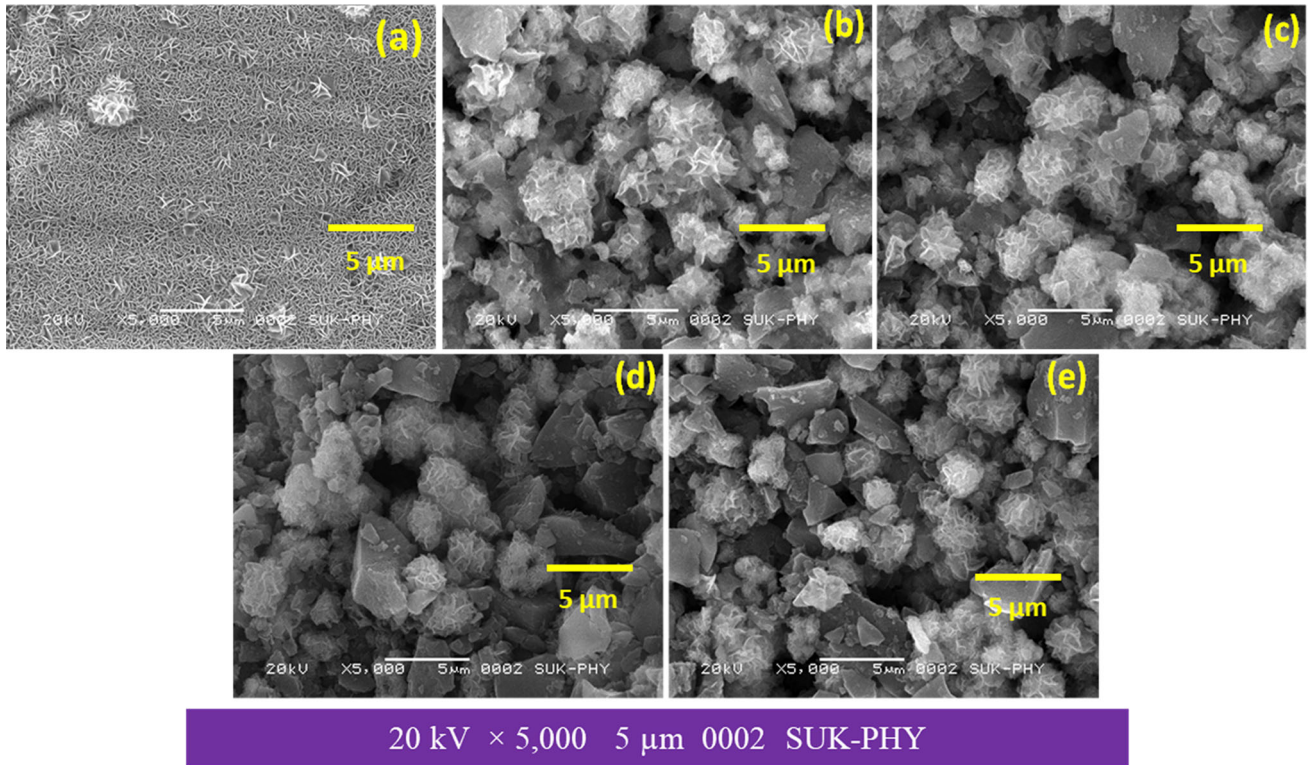
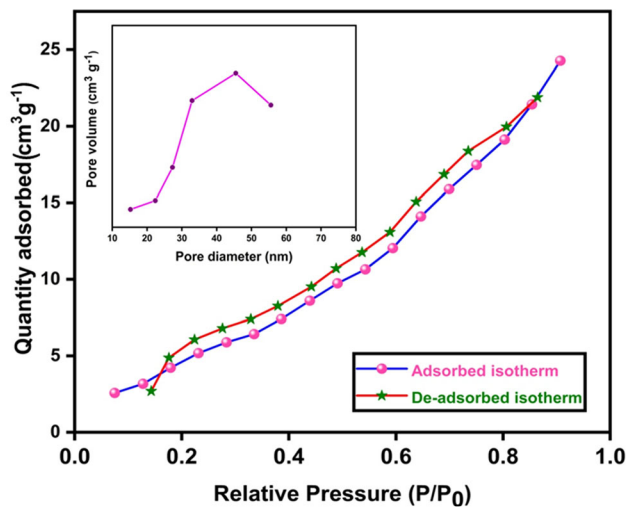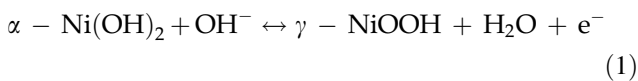**Fig. 3** SEM images of **a** pure α-Ni(OH)₂ film, **b** NAC-1, **c** NAC-2, **d** NAC-3, and **e** NAC-4

Fig. 4 BET isotherm plots (the inset is BJH pore distribution) of the NAC-2

$$\alpha - Ni(OH)_2 + OH^- \leftrightarrow \gamma - NiOOH + H_2O + e^-$$

$$(1)$$

The anodic peak reveals the oxidation reaction of α-Ni(OH)₂ to γ-NiOOH, while the cathodic peak reveals the reduction reaction. The electroactive ions in the electrolyte are intercalated to the electrode surface at the time of charging, while these ions are intercalated into the electrolyte during the discharging process. The porous nature of the electrode surface facilitates the ion transfer process.

The C_{sp} of pure α-Ni(OH)₂ and composite electrodes decreases with an increase in the scan rate. With an increase in the scan rate, the electrolyte ions access only the external surface of the electrode material. However, the electrolyte ions cannot utilize the entire active sites of the electrode material. Therefore, the decrement in the C_{sp} of pure and composite electrodes with an increasing scan rate is because of the reduction in the utilization rate of the working electrodes [29]. The values of C_{sp} of pure α-Ni(OH)₂ and NAC-1, NAC-2, NAC-3, and NAC-4 films are determined at a scan rate of 10 mVs⁻¹ by the following Eq. (2) [29–33] and are listed in Table 1.

$$C_{sp} = \frac{\int i dv}{mV(\Delta V)} \tag{2}$$

where $\int i \, dv$ assigned the area under CV curve between the potential range, m (g) is the mass of the active material onto the substrate, V (mV s⁻¹) is the scan rate, and ΔV (V) is the potential window. Moreover, from Fig. 5b–e it is seen that, the
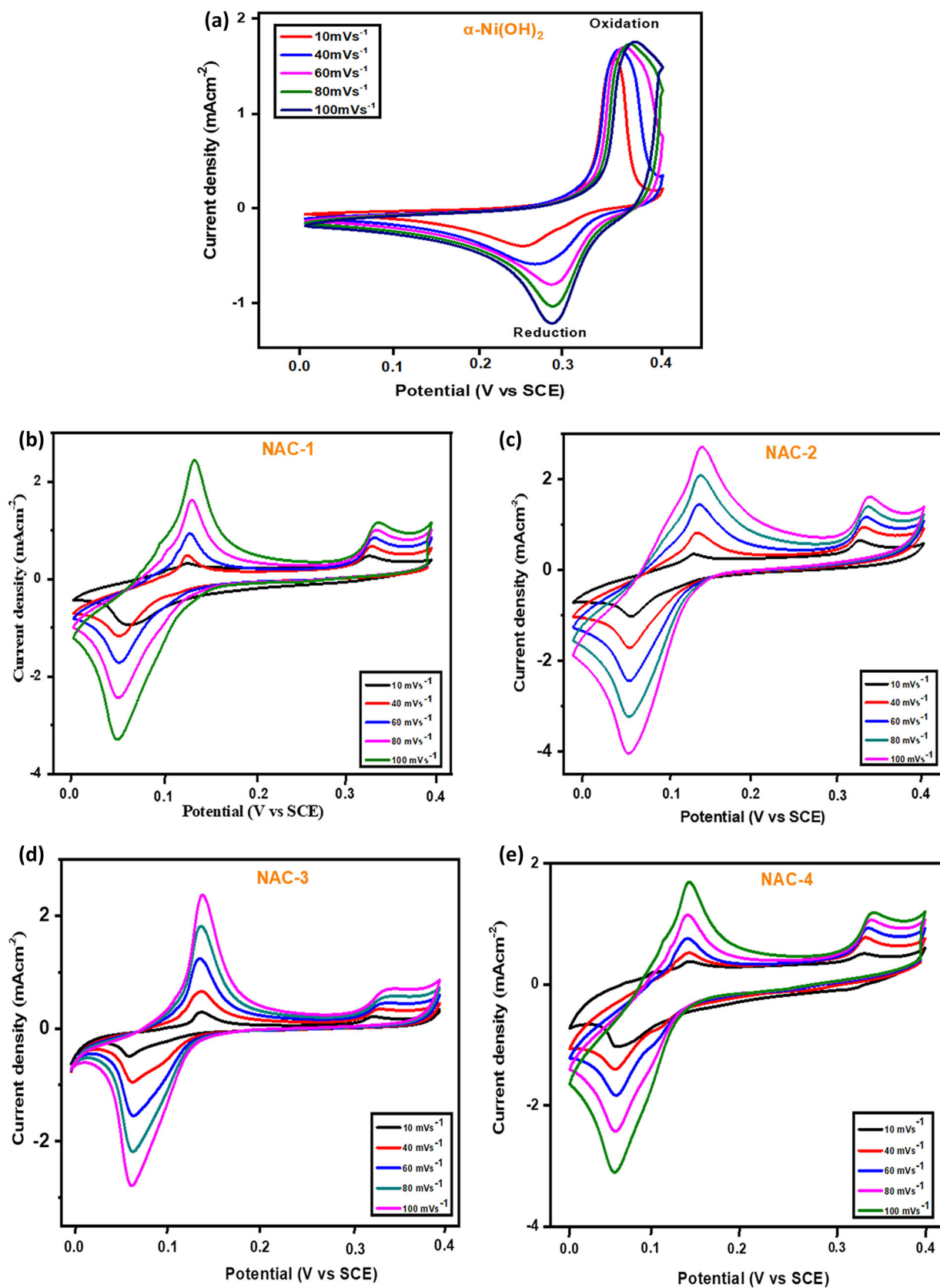
🖄 Springer

Fig. 5 Cyclic voltammograms of **a** pure α-Ni(OH)$_2$ film, **b** NAC-1, **c** NAC-2, **d** NAC-3, and **e** NAC-4 at different scan rates

Springer

Table 1 Electrochemical performance evaluated for pure α-Ni(OH)$_2$ film and α-Ni(OH)$_2$–AC composite films

Working Electrode	Sp. Capacitance by CV (Fg^{-1})	Sp. Capacitance by CD (Fg^{-1})	Specific energy (Wh kg^{-1})	Specific power (kWkg^{-1})
α-Ni(OH)$_2$	298	280	10.20	2.42
NAC-1	394	386	14.10	3.05
NAC-2	436	427	16.12	3.90
NAC-3	380	368	13.20	2.88
NAC-4	322	320	11.97	2.65

voltammetric current of α-Ni(OH)$_2$–AC composite films is found to be more than pure α-Ni(OH)$_2$ film, which can be ascribed to the presence of AC in the composite [34]. The expanse of the CV curve of NAC-2 is more than pure α-Ni(OH)$_2$, NAC-1, NAC-3, and NAC-4. Therefore, the incorporation of AC in pure α-Ni(OH)$_2$ for the composite NAC-2 provided enhanced C_{sp} than pure α-Ni(OH)$_2$ and other composite films. The improvement in the C_{sp} of NAC-2 can be ascribed to a large surface area and pore size distribution of the NAC-2 [5]. The increase in the concentration of AC for NAC-3 and NAC-4 composites decreases the voltammetric current. Because of this, the C_{sp} of NAC-3 and NAC-4 decreases.

From the CV analysis, it is inferred that, an increase in the concentration of AC in pure α-Ni(OH)$_2$ leads to loss of pseudocapacitive behavior of nickel hydroxide and switches the charge storage mechanism of electrode material from pseudocapacitive nature to EDLC. The NAC-2 exhibits a maximum C_{sp} of 436 Fg^{-1}.

3.5.2 Galvanostatic charge–discharge (GCD) studies

Figure 6 displays the GCD plots of pure α-Ni(OH)$_2$ film, NAC-1, NAC-2, NAC-3, and NAC-4, at a constant current density of 1 mA cm^{-2}. The GCD analysis reflects the imperfect non-triangular nature of the curves, which signifies the typical pseudocapacitive nature of electrode materials because of faradic redox reactions and is consistent with the CV study [14, 35]. The values of C_{sp}, specific energy (E), and specific power (P) of the pure and composite electrodes are determined from the following Eqs. (3–5), respectively [29–33], and are presented in Table 1.
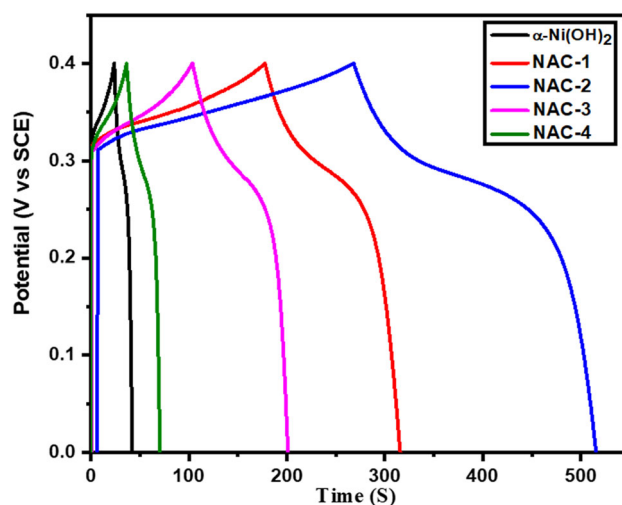

Fig. 6 Galvanostatic charge–discharge curves of pure α-Ni(OH)$_2$ film, NAC-1, NAC-2, NAC-3, and NAC-4 at a constant current density of 1 mA cm^{-2}

$$C_{sp} = \frac{I}{m\frac{\Delta V}{\Delta t}} \tag{3}$$

$$E = 0.5\, C_{sp}(\Delta V)^2 \tag{4}$$

$$P = \frac{E}{\Delta t} \tag{5}$$

where I (mA) is the current density, m (g) is the mass of the active material, Δt (sec) and ΔV (V) are the discharge time and potential window, respectively. The NAC-2 shows better C_{sp} of 427 Fg^{-1} as compared to other electrodes, because of the large discharge time.

Vijayakumar and Muralidharan [35] reported the energy density and power density of Ni(OH)$_2$/AC asymmetric device as 1.83 Wh kg^{-1} and 2.99 kW kg^{-1}, respectively. Chang et al. [36] reported the specific energy of 0.06 Wh kg^{-1} and the specific power of 0.97 kWkg^{-1} for nickel–cobalt oxide/AC nanocomposites. Su et al. [37] demonstrated the

🖄 Springer

energy density of 21.8 Wh kg^{-1} and power density of 0.66 kWkg^{-1} for Ni(OH)$_2$@3D–Ni/AC electrodes. Huang et al. [38] fabricated AC//β–Ni(OH)$_2$/Ni-foam asymmetric supercapacitors and reported energy density of 36.2 Wh kg^{-1}, with power density of 0.10 kW kg^{-1}.

The values of specific energy and specific power determined for NAC-2 electrode are 16.12 Wh kg^{-1} and 3.90 kW kg^{-1}, respectively, which indicate promising electrochemical performance of the NAC-2 composite electrodes.

The long-term cycle stability of the electrode material is an important parameter, which determines the practical applications of supercapacitors. The cyclic stability study of pure α-Ni(OH)$_2$ and NAC-2 is evaluated through the CV. Figure 7 shows the cyclic stability of pure α-Ni(OH)$_2$ electrode and NAC-2 composite electrode at 100 mVs^{-1} for 1500 cycles. For 1500 cycles, the capacitance retention rate of NAC-2 is 81%, whereas the capacitance retention rate of pure α-Ni(OH)$_2$ is 70%. The enhancement in the conductivity of NAC-2 may be responsible for the high-capacitance retention of the NAC-2 electrode. Moreover, for α-Ni(OH)$_2$ and NAC-2 electrodes, the capacitive loss exhibited is 10% after 500 cycles and 1000 cycles, respectively, which signify that the α-Ni(OH)$_2$–AC composite electrode shows remarkable rate ability in 1 M KOH electrolyte. Therefore, α-Ni(OH)$_2$–AC electrodes are the competent candidates for the fabrication of efficient electrochemic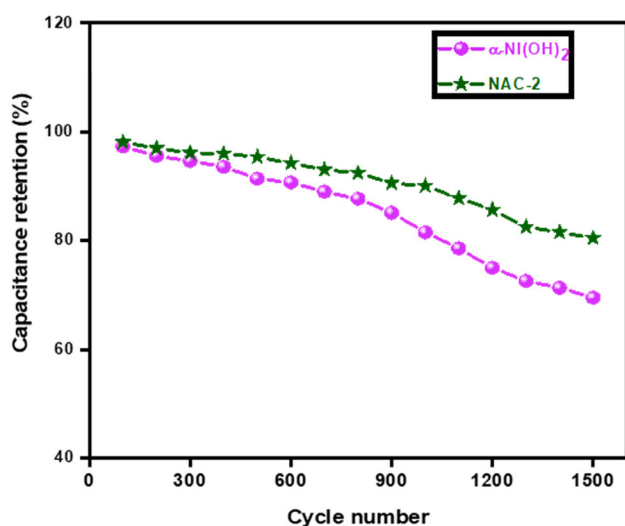al supercapacitors. Table 2 shows the comparison of specific capacitance and cyclic stability of Ni(OH)$_2$-based electrode materials from the present work with other research groups.

3.5.3 Electrochemical impedance spectroscopy (EIS) analysis

The EIS study of α-Ni(OH)$_2$ and α-Ni(OH)$_2$–AC composite electrodes was carried out over a frequency range of 10–1 MHz. The Nyquist plots of pure α-Ni(OH)$_2$ and NAC-1, NAC-2, NAC-3, and NAC-4 electrodes are shown in Fig. 8a and b, respectively. At the high-frequency region, the small diameter of semicircle represents the lowest value of charge transfer resistance (R_{ct}), and the intercept of the plot with the real axis (Z') represents the equivalent series resistance (ESR) and is denoted by R_s [41]. From the Nyquist plots, it is observed that the pure α-Ni(OH)$_2$ electrode and α-Ni(OH)$_2$–AC composite electrodes show depressed semicircle in the high-frequency region and an inclined straight line with the finite slope in the low-frequency region. In Fig. 8a, for the α-Ni(OH)$_2$ electrode, a semicircle with a large diameter is observed, which is followed by an inclined straight line, whereas in Fig. 8b, for α-Ni(OH)$_2$–AC composite electrodes, the diameters of the semicircles get reduced, and the slope of straight lines gets increased.

The inset of Fig. 8b shows the equivalent electric circuit used for fitting the Nyquist plots. The different parameters such as R_s, R_{ct}, Warburg diffusion resistance (Zw), and double layer capacitance (C_P) evaluated from the EIS study are listed in Table 3. The determined values of R_s, R_{ct}, and Zw are 1.19 Ω, 14 Ω, and 7.8 Ω, for NAC-2, 2.69 Ω, 42 Ω, and 27.2 Ω, for α-Ni(OH)$_2$, 1.92 Ω, 22 Ω, and 12.3 Ω, for NAC-1, 2.02 Ω, 28 Ω, and 18.2 Ω, for NAC-3, and 2.10 Ω, 38 Ω, and 24.5 Ω, for NAC-4, respectively. The better electrochemical performance of NAC-2 electrode over the other electrodes in 1 M KOH electrolyte can be attributed to comparatively lower values of R_s, R_{ct}, and Zw of the NAC-2 electrode.

4 Conclusions

Chemically synthesized α-Ni(OH)$_2$ and α-Ni(OH)$_2$–AC composite films showed noteworthy electrochemical activities in 1 M KOH electrolyte. The FT-IR analysis reflected the formation of α-Ni(OH)$_2$–AC

Fig. 7 Cyclic stability of pure α-Ni(OH)$_2$ film and NAC-2 at 100 mV s^{-1} for 1500 cycles

🍃 Springer

Table 2 Comparison of specific capacitance and cyclic stability of Ni(OH)$_2$-based electrode material from the present work with other research groups

| Working Electrode	Current collector	Synthesis Method	Electrolyte	Specific capacitance (Fg^{-1})	Capacitance retention/ after cycles	References
Ni(OH)$_2$ nanosheets	Titanium foil	Hydrothermal	1 M KOH	180	76%/1500	[14]
Mesoporous nickel hydroxide	Indium doped tin oxide (ITO)	Layer-by-layer deposition (LbL)	1 M LiCl	85	45%/800	[15]
α-Ni(OH)$_2$	Graphite sheet	Green synthesis	2 M KOH	291	82%/500	[35]
NiO	Nickel foam	Molten-salt synthesis	2 M KOH	72.2	–	[39]
Ni(OH)$_2$	Stainless steel	Electrodeposition	1 M NaOH	113.8	40.7%/1000	[40]
NAC-2	Stainless steel	Chemical precipitation	1 M KOH	436	81%/1500	This work
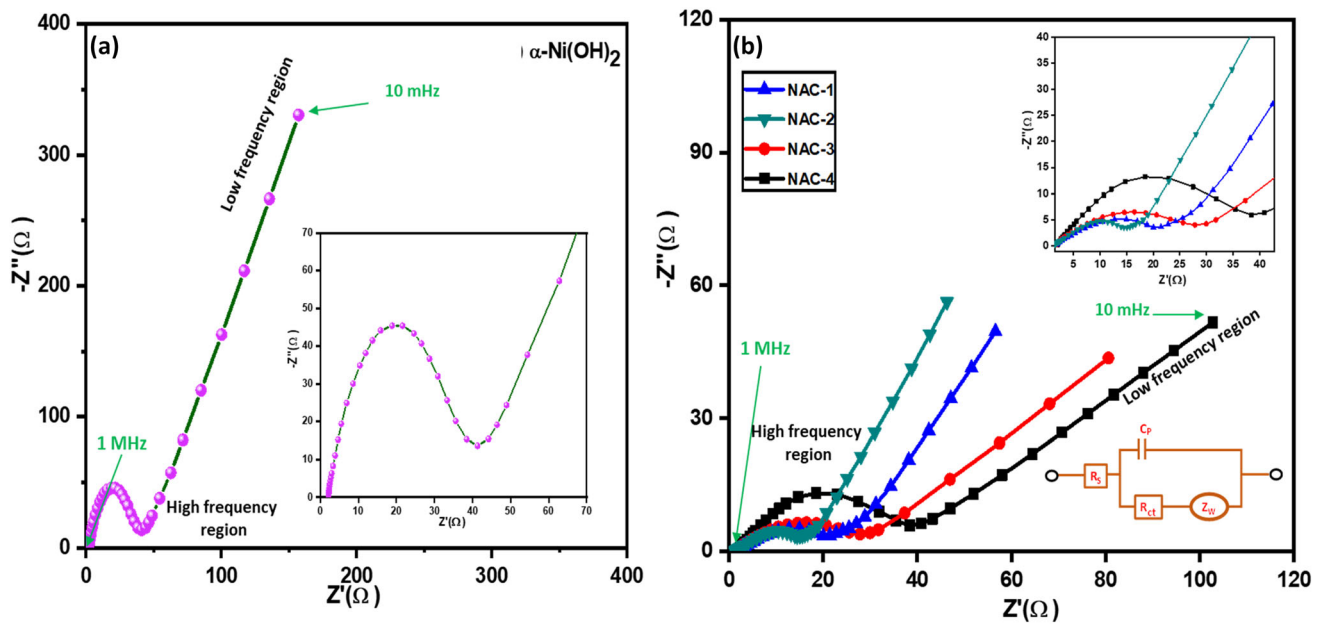
Fig. 8 Nyquist plot of **a** pure α-Ni(OH)$_2$ film **and b** α-Ni(OH)$_2$–AC composite films NAC-1, NAC-2, NAC-3, and NAC-4

Table 3 The fitted equivalent electric circuit parameters of the α-Ni(OH)$_2$, NAC-1, NAC-2, NAC-3, and NAC-4

Working Electrode	R_S (Ω)	R_{Ct} (Ω)	Z_W (Ω)	C_p (F)
α-Ni(OH)$_2$	2.69	42	27.2	0.28
NAC-1	1.92	22	12.3	0.43
NAC-2	1.19	14	7.8	0.54
NAC-3	2.02	28	18.2	0.39
NAC-4	2.10	38	24.5	0.32

composite. The morphological study revealed the porous nature of α-Ni(OH)$_2$, and α-Ni(OH)$_2$–AC composite films comprising sheets and microflowers, which is suitable for rapid intercalation–deintercalation of electrolyte ions at the electrode–electrolyte interface. The NAC-2 electrode showed good electrochemical properties such as specific capacitance of 436 Fg^{-1}, 81% of capacitance retention rate after 1500 cycles, specific energy of 16.12 Wh kg^{-1}, and specific power of 3.90 kW kg^{-1}.

The present results suggest a cost-effective approach for fabricating the efficient electrochemical capacitors rooted in non-toxic and copious materials.

Acknowledgements

References

1. G. Wang, L. Zhang, J. Zhang, A review of electrode materials for electrochemical supercapacitors. Chem. Soc. Rev. **41**, 797 (2012)

2. L. Jiao, X. Pan, Y. Xi, J. Li, J. Cao, Q. Guo, W. Han, A facile synthesis of self-assembling reduced graphene oxide/cobalt carbonate hydroxide papers for high-performance supercapacitor applications. J. Mater. Sci. Mater. Electron. **30**, 159 (2019)

3. L. Gong, X. Liu, L. Su, Facile solvothermal synthesis Ni(OH)$_2$ nanostructure for electrochemical capacitors. J. Inorg. Organomet. Polym. Mater. **21**, 866 (2011)

4. L.L. Zhang, X.S. Zhao, Carbon-based materials as supercapacitor electrodes. Chem. Soc. Rev. **38**, 2520 (2009)

5. D. Qu, H. Shi, Studies of activated carbons used in double-layer capacitors. J. Power Sources **74**, 99 (1998)

6. E. Frackowiak, Carbon materials for supercapacitor application. Phys. Chem. Chem. Phys. **9**, 1774 (2007)

7. S. Faraji, F.N. Ani, The development supercapacitor from activated carbon by electroless plating—a review. Renew. Sustain. Energy Rev. **42**, 823 (2015)

8. J.W. Wang, Y. Chen, B.Z. Chen, A synthesis method of MnO$_2$/activated carbon composite for electrochemical supercapacitors. J. Electrochem. Soc. **162**, A1654 (2015)

9. R. Madhu, V. Veeramani, S.M. Chen, A. Manikandan, A.Y. Lo, Y.L. Chueh, Honeycomb-like porous carbon–cobalt oxide nanocomposite for high-performance enzymeless glucose sensor and supercapacitor applications. ACS Appl. Mater. Interfaces **7**, 15812 (2015)

10. Y.F. Su, W.U. Feng, L.Y. Bao, Z.H. Yang, RuO$_2$/activated carbon composites as a positive electrode in an alkaline electrochemical capacitor. New Carbon Mater. **22**, 53 (2007)

11. M. Selvakumar, D.K. Bhat, A.M. Aggarwal, S.P. Iyer, G. Sravani, Nano ZnO-activated carbon composite electrodes for supercapacitors. Phys. B **405**, 2286 (2010)

12. S.D. Dhas, P.S. Maldar, M.D. Patil, A.B. Nagare, M.R. Waikar, R.G. Sonkawade, A.V. Moholkar, Synthesis of NiO nanoparticles for supercapacitor application as an efficient electrode material. Vacuum **181**, 109646 (2020)

13. Q. Huang, X. Wang, J. Li, C. Dai, S. Gamboa, P.J. Sebastian, Nickel hydroxide/activated carbon composite electrodes for electrochemical capacitors. J. Power Sources **164**, 425 (2007)

14. K.S. Bhat, H.S. Nagaraja, Morphology-dependent electrochemical performances of nickel hydroxide nanostructures. Bull. Mater. Sci. **42**, 265 (2019)

15. J. Chang, M. Park, D. Ham, S.B. Ogale, R.S. Mane, S.H. Han, Liquid-phase synthesized mesoporous electrochemical supercapacitors of nickel hydroxide. Electrochem. Acta. **53**, 5016 (2008)

16. J.H. Park, O.O. Park, K.H. Shin, C.S. Jin, J.H. Kim, An electrochemical capacitor based on a Ni(OH)$_2$/activated carbon composite electrode. Electrochem. Solid-State Lett. **5**, H7 (2002)

17. G.R. Fu, Z.A. Hu, L.J. Xie, X.Q. Jin, Y.L. Xie, Y.X. Wang, Z.Y. Zhang, Y.Y. Yang, H.Y. Wu, Electrodeposition of nickel hydroxide films on nickel foil and its electrochemical performances for supercapacitor. Int. J. Electrochem. Sci. **4**, 1052 (2009)

18. S. Tang, L. Sui, Z. Dai, Z. Zhu, H. Huangfu, High supercapacitive performance of Ni (OH)$_2$/XC-72 composite prepared by microwave-assisted method. Rsc Adv. **5**, 43164 (2015)

19. G.S. Gund, D.P. Dubal, N.R. Chodankar, J.Y. Cho, P. Gomez-Romero, C. Park, C.D. Lokhande, Low-cost flexible supercapacitors with high-energy density based on nanostructured MnO$_2$ and Fe$_2$O$_3$ thin films directly fabricated onto stainless steel. Sci. Rep. **5**, 12454 (2015)

20. M. El-Kemary, N. Nagy, I. El-Mehasseb, Nickel oxide nanoparticles: synthesis and spectral studies of interactions with glucose. Mater. Sci. Semicond. Proc. **16**, 1747 (2013)

21. J.W. Lee, J.M. Ko, J.D. Kim, Hierarchical microspheres based on α-Ni(OH)2 nanosheets intercalated with different anions: synthesis, anion exchange, and effect of intercalated anions on electrochemical capacitance. J. Phys. Chem. C **115**, 19445 (2011)

22. L.X. Yang, Y.J. Zhu, H. Tong, Z.H. Liang, L. Li, L. Zhang, Hydrothermal synthesis of nickel hydroxide nanostructures in mixed solvents of water and alcohol. J. Solid State Chem. **180**, 2095 (2007)

23. H.B. Li, M.H. Yu, F.X. Wang, P. Liu, Y. Liang, J. Xiao, C.X. Wang, Y.X. Tong, G.W. Yang, Amorphous nickel hydroxide nanospheres with ultrahigh capacitance and energy density as

electrochemical pseudocapacitor materials. Nat. Commun. **4**, 1894 (2013)

24. X. Xie, L. Gao, Characterization of a manganese dioxide/carbon nanotube composite fabricated using an in situ coating method. Carbon **45**, 2365 (2007)

25. S. Gong, Q. Cao, L. Jin, C. Zhong, X. Zhang, Electrodeposition of three-dimensional $Ni(OH)_2$ nanoflakes on partially crystallized activated carbon for high-performance supercapacitors. J. Solid State Electrochem. **20**, 619 (2016)

26. L. Fan, L. Tang, H. Gong, Z. Yao, R. Guo, Carbonnanoparticles encapsulated in hollow nickel oxides for supercapacitor application. J. Mater. Chem. **22**, 16376 (2012)

27. M.S. Wu, Y.A. Huang, C.H. Yang, Capacitive behavior of porous nickel oxide/hydroxide electrodes with interconnected nanoflakes synthesized by anodic electrodeposition. J. Electrochem. Soc. **155**, A798 (2008)

28. J.W. Lang, L.B. Kong, W.J. Wu, M. Liu, Y.C. Luo, L. Kang, A facile approach to the preparation of loose-packed $Ni(OH)_2$ nanoflake materials for electrochemical capacitors. J. Solid State Electrochem. **13**, 333 (2009)

29. M.R. Waikar, A.S. Rasal, N.S. Shinde, S.D. Dhas, A.V. Moholkar, M.D. Shirsat, S.K. Chakarvarti, R.G. Sonkawade, Electrochemical performance of polyaniline based symmetrical energy storage device. Mat. Sci. Semicon. Proc. **120**, 105291 (2020)

30. X. Zhang, J. Wang, X. Ji, Y. Sui, F. Wei, J. Qi, Q. Meng, Y. Ren, Y. He, Nickel/cobalt bimetallic metal-organic frameworks ultrathin nanosheets with enhanced performance for supercapacitors. J. Alloys Compd. **825**, 154069 (2020)

31. Y. He, X. Zhang, S. Wang, J. Meng, Y. Sui, F. Wei, J. Qi, Q. Meng, Y. Ren, D. Zhuang, Rubik's cube-like Ni_3S_4/CuS_2 nanocomposite for high-performance supercapacitors. J. Alloys Compd. **847**, 156312 (2020)

32. S. Gao, Y. Sui, F. Wei, J. Qi, Q. Meng, Y. He, Facile synthesis of cuboid Ni-MOF for high-performance supercapacitors. J. Mater. Sci. **53**, 6807–6818 (2018)

33. S. Gao, Y. Sui, F. Wei, J. Qi, Q. Meng, Y. Ren, Y. He, Dandelion-like nickel/cobalt metal-organic framework based electrode materials for high performance supercapacitors. J. Colloid Interface Sci. **531**, 83 (2018)

34. D.P. Dubal, G.S. Gund, C.D. Lokhande, R. Holze, Decoration of sponge-like $Ni(OH)_2$ nanoparticles onto MWCNTs using an easily manipulated chemical protocol for supercapacitors. ACS Appl. Mater. Interfaces **5**, 2446 (2013)

35. S. Vijayakumar, G. Muralidharan, Electrochemical supercapacitor behaviour of α-$Ni(OH)_2$ nanoparticles synthesized via green chemistry route. J. Electroanal. Chem. **727**, 53 (2014)

36. S.K. Chang, Z. Zainal, K.B. Tan, N.A. Yusof, W.M.D.W. Yusoff, S.R.S. Prabaharan, Nickel-cobalt oxide/activated carbon composite electrodes for electrochemical capacitors. Curr. Appl. Phys. **12**, 1421 (2012)

37. Y.Z. Su, K. Xiao, N. Li, Z.Q. Liu, S.Z. Qiao, Amorphous $Ni(OH)_2$ @ three-dimensional Ni core–shell nanostructures for high capacitance pseudocapacitors and asymmetric supercapacitors. J. Mater. Chem. A **2**, 13845 (2014)

38. J. Huang, P. Xu, D. Cao, X. Zhou, S. Yang, Y. Li, G. Wang, Asymmetric supercapacitors based on β-$Ni(OH)_2$ nanosheets and activated carbon with high energy density. J. Power Sources **246**, 371 (2014)

39. Y.Z. Zheng, M.L. Zhang, Preparation and electrochemical properties of nickel oxide by molten-salt synthesis. Mater. Lett. **61**, 3967 (2007)

40. J.H. Shendkar, V.V. Jadhav, P.V. Shinde, R.S. Mane, C. O'Dwyer, Hybrid composite polyaniline-nickel hydroxide electrode materials for supercapacitor applications. Heliyon **4**, 801 (2018)

41. Y. Zhou, J. Jin, L. Chen, Y. Zhu, B. Xu, Open-ended carbon microtubes/carbon nanotubes for high-performance supercapacitors. Mater. Lett. **241**, 80 (2019)

Terms and Conditions

Springer Nature journal content, brought to you courtesy of Springer Nature Customer Service Center GmbH ("Springer Nature").

Springer Nature supports a reasonable amount of sharing of research papers by authors, subscribers and authorised users ("Users"), for small-scale personal, non-commercial use provided that all copyright, trade and service marks and other proprietary notices are maintained. By accessing, sharing, receiving or otherwise using the Springer Nature journal content you agree to these terms of use ("Terms"). For these purposes, Springer Nature considers academic use (by researchers and students) to be non-commercial.

These Terms are supplementary and will apply in addition to any applicable website terms and conditions, a relevant site licence or a personal subscription. These Terms will prevail over any conflict or ambiguity with regards to the relevant terms, a site licence or a personal subscription (to the extent of the conflict or ambiguity only). For Creative Commons-licensed articles, the terms of the Creative Commons license used will apply.

We collect and use personal data to provide access to the Springer Nature journal content. We may also use these personal data internally within ResearchGate and Springer Nature and as agreed share it, in an anonymised way, for purposes of tracking, analysis and reporting. We will not otherwise disclose your personal data outside the ResearchGate or the Springer Nature group of companies unless we have your permission as detailed in the Privacy Policy.

While Users may use the Springer Nature journal content for small scale, personal non-commercial use, it is important to note that Users may not:

1. use such content for the purpose of providing other users with access on a regular or large scale basis or as a means to circumvent access control;

2. use such content where to do so would be considered a criminal or statutory offence in any jurisdiction, or gives rise to civil liability, or is otherwise unlawful;

3. falsely or misleadingly imply or suggest endorsement, approval , sponsorship, or association unless explicitly agreed to by Springer Nature in writing;

4. use bots or other automated methods to access the content or redirect messages

5. override any security feature or exclusionary protocol; or

6. share the content in order to create substitute for Springer Nature products or services or a systematic database of Springer Nature journal content.

In line with the restriction against commercial use, Springer Nature does not permit the creation of a product or service that creates revenue, royalties, rent or income from our content or its inclusion as part of a paid for service or for other commercial gain. Springer Nature journal content cannot be used for inter-library loans and librarians may not upload Springer Nature journal content on a large scale into their, or any other, institutional repository.

These terms of use are reviewed regularly and may be amended at any time. Springer Nature is not obligated to publish any information or content on this website and may remove it or features or functionality at our sole discretion, at any time with or without notice. Springer Nature may revoke this licence to you at any time and remove access to any copies of the Springer Nature journal content which have been saved.

To the fullest extent permitted by law, Springer Nature makes no warranties, representations or guarantees to Users, either express or implied with respect to the Springer nature journal content and all parties disclaim and waive any implied warranties or warranties imposed by law, including merchantability or fitness for any particular purpose.

Please note that these rights do not automatically extend to content, data or other material published by Springer Nature that may be licensed from third parties.

If you would like to use or distribute our Springer Nature journal content to a wider audience or on a regular basis or in any other manner not expressly permitted by these Terms, please contact Springer Nature at

onlineservice@springernature.com